COMPUTER GRAPHICS AND IMAGE PROCESSING 6, 513–537 (1977)

Iterative Three-Dimensional Image Reconstruction from Tomographic Projections*

JAMES G. COLSHER[1]

Biomedical and Environmental Research Division, Lawrence Livermore Laboratory, Livermore, California 94550

Received June 16, 1976

Four algorithms are adapted to perform direct three-dimensional reconstruction from projections. The algorithms considered are summation, the Algebraic Reconstruction Technique (ART), the Simultaneous Iterative Reconstruction Technique (SIRT), and the Iterative Least Squares Technique (ILST). The concept of tomographic projections is introduced and shown to greatly simplify the calculations. This work represents the first time that these iterative algorithms have been applied to projections other than coaxial. The methods developed can be of benefit in electron microscopy, holographic interferometry, and nuclear medicine. To evaluate these methods an experimental investigation is carried out using computer-generated synthetic images. Using SIRT, direct 3-D reconstruction is shown to be superior to serial 2-D reconstruction from coaxial projections when the range of viewing angles is limited. The number of projections required for adequate reconstruction is also considered. Finally, the performance of the algorithms is compared with respect to overall similarity of the reconstruction to the original test object, effects of noise, and computer time and memory requirements.

1. INTRODUCTION

The problem of reconstructing three-dimensional images from projections has arisen in fields as diverse as electron microscopy, radiology, and radioastronomy. Various techniques have been proposed to solve this problem; the earliest was developed by Radon in 1917 [1]. Good reviews of the subject are given by Budinger and Gullberg [2] and Gordon and Herman [3]. Most of the techniques presented to date are actually two-dimensional procedures for reconstructing a series of parallel planes from multiple one-dimensional projections. For these methods, coaxial projection data are obtained by rotating the object about a fixed axis so that object planes perpendicular to the axis project into a line. The corresponding lines in the different projections are used to reconstruct each plane

* This work was performed in partial fulfillment of the requirements for the degree of Doctor of Philosophy in the Department of Biomedical Engineering, University of Pennsylvania, and was performed under the auspices of the U.S. Energy Research and Development Administration, Contract No. W-7405-ENG-48. Portions of the work were presented at the *Topical Meeting on Image Processing for 2-D and 3-D Reconstruction from Projections: Theory and Practice in Medicine and the Physical Sciences* held at Stanford University, August 4–7, 1975.

[1] Present address: Searle Radiographics, 200 Nuclear Drive, Des Plaines, Illinois 60018.

ISSN 0146-664X

in turn. Computationally, the problem is thus reduced from three dimensions to two. The planes are then stacked to get the three-dimensional reconstruction. Other methods of data collection can be used, but they do not allow for reduction of the dimensionality of the reconstruction problem as do the coaxial projections. For these other methods the entire three-dimensional reconstruction must be calculated simultaneously; this poses complex mathematical and computational problems. However, true 3-D reconstruction is of interest because it increases the flexibility of data acquisition and may be advantageous in situations such as electron microscopy where the range of viewing angles is limited.

The prime objective of this work is the modification of iterative algebraic algorithms to perform true 3-D reconstructions from projections; the algorithms considered are summation, the Algebraic Reconstruction Technique (ART) [4], the Simultaneous Iterative Reconstruction Technique (SIRT) [5], and the Iterative Least Squares Technique (ILST) [6]. The concept of tomographic projections is introduced. These projections are useful because they simplify the calculations and because there are many devices that can collect data in this manner. For example, the data-collection methods of Hart [7] in electron microscopy essentially produce tomographic projections. In nuclear medicine, the rotating slant-hole collimator camera and the multiwire proportional-chamber positron camera [8] both produce tomographic projections although in the latter case some preprocessing of the data is necessary. In holographic interferometry, the thin-beam reconstruction method [9] can also be used.

A further goal is an experimental evaluation of the 3-D reconstruction procedure using computer-generated synthetic images. Although it can be shown that iterative algorithms are all gradient methods [10] this does little to predict their performance and a general theory does not exist. Consequently, an experimental investigation was undertaken. This consisted of building test objects and taking their projections, applying the various algorithms to the projection data, and then comparing the reconstructions with the original, The first experiment was designed to ascertain the advantages, if any, of 3-D reconstruction over serial 2-D reconstruction. Using SIRT, reconstructions from linear tomographic (coaxial) projections are compared with reconstructions from circular tomographic projections. In the second experiment, the effect of varying the number of views on the performance of SIRT is evaluated. Finally, the four algorithms are compared with respect to resolution and noise characteristics.

2. THE RECONSTRUCTION PROBLEM

Images formed by penetrating radiation represent a projection of densities. By using an external source of radiation, one obtains a transmission picture (projection) of the 3-D object onto a surface such as the film of an x-ray or electron micrograph. Considered mathematically, a point on the image represents the line integral of a density function. Thus, examining an object from many views effectively generates sets of equations. The reconstruction problem is to estimate the internal density distribution from these equations.

Reconstruction techniques can be grouped into three broad classes. In the

first, called tomography or summation, the rays through each point are simply added to obtain an estimate of the density at the point. The second class formulates the problem in terms of integral equations and employs Fourier transforms, convolutions, or orthogonal expansions [12]. The third class uses algebraic approaches and involves matrix inversion or iterative approximation. Each of these classes is now discussed briefly in turn.

Tomography is the oldest and most widely used technique for imaging a plane in a three-dimensional body. In radiological applications, the source and film pivot about a selected plane during exposure so that the image of this plane, the tomographic plane, remains stationary on the moving film while the images of other planes are displaced and blurred. Grant [13] proposed the use of a sampled system in which a series of images are projected onto separate films, thus permitting the reconstruction of all object planes. The central tomographic plane is obtained by superimposing all the films. Other planes are obtained by displacing the various radiographs relative to each other and then superimposing them. The application of tomography in electron microscopy has been described by Hart [7] and Hart and Yoshiyama [14]. Images are obtained by tilting the specimen in the electron microscope and taking transmission micrographs of the same area along different directions.

Several methods of reconstruction based on integral equation formulations have been proposed. As noted earlier, most of these methods are based on two-dimensional integral equations and hence require coaxial projections. However, some of these 2-D techniques can be modified to apply to the 3-D problem. In theory, Fourier techniques [12] can easily be extended, since the projection theorem holds. This theorem states that the 2-D Fourier transform of the projection is identical to the corresponding central section of the 3-D transform of the object. Crowther, Klug, and coworkers have employed Fourier reconstruction extensively in electron microscopy for the reconstruction of symmetrical objects such as viruses [15]. However, the extension to nonsymmetric particles presents technical problems, in particular the registration of different views.

In the algebraic or iterative techniques, the object is partitioned into cells. The density within each cell is assumed uniform and the measure of the line integral along a single ray is related to the densities through a linear relationship. This results in a set of linear equations, one for each ray. Estimates of the cell density values are made and the linear equations are used to calculate projection data. Errors between calculated and measured projection data are then used to modify the cell density values.

These iterative techniques appear to be the most promising for reconstruction from tomographic projections. Since they have been formulated in terms of linear algebra their extension to 3-D reconstruction requires only a description of the path of a ray through a volume. Some work in this area has already been done by other investigators. Radulovic and Vest [16] presented the results for the "grid" method, which involves a least squares solution. Schmidlin [17] presented a iterative algorithm, referred to by Budinger as the Simultaneous Iterative Geometric Mean Technique. It was not used in our investigation

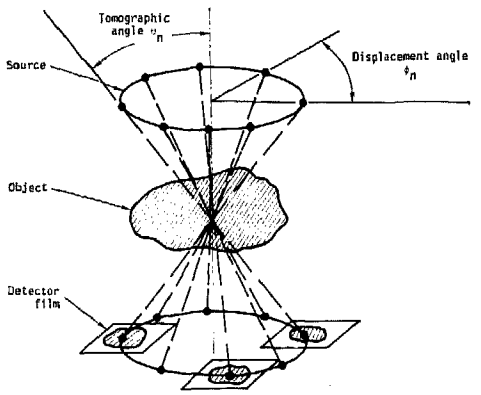

FIG. 1. The projection geometry is indicated for circular tomographic projections. The displacement angle ϕ_n and the tomographic angle θ_n correspond to the angles normally defined in a spherical coordinate system.

because it involved considerable multiplication, a computationally expensive operation.

3. ALGORITHMS

In this section the pertinent quantities are defined and the algorithms are explained. The reconstruction volume is divided into individual cells or voxels (volume cells) $D(i, j, k)$ where $i = 1, \ldots, I$; $j = 1, \ldots, J$, and $k = -K, \ldots, K$ divide the volume into $2K + 1$ plane sections of I by J cells each. For the symmetry or center plane $k = 0$ and in general $I = J$. D represents the density and is assumed constant within a voxel.

A projection is determined by two angles: the tomographic angle, θ_n, and the displacement angle, ϕ_n (Fig. 1). These correspond to the angles normally defined in a spherical coordinate system. In general there are N projections, each divided into pixels (picture cells) $P(l, m, n)$ in which $l = 1, \ldots, L$, $m = 1, \ldots, M$, and $n = 1, \ldots, N$. Each pixel corresponds to the measured projection density along a particular ray. Thus, there are $L \times M \times N$ rays. These projections are defined so that they are parallel to the plane sections or, to state it another way, perpendicular to the k axis. Further, the projection coordinates are defined so that they correspond to those of the symmetry plane; $i = l$ and $j = m$ for $k = 0$. The coordinates of any voxel are related to the projection coordinates by the following equations, where integer arithmetic is assumed.

$$\begin{aligned} l &= i - k \tan \theta_n \cos \phi_n, \\ m &= j - k \tan \theta_n \sin \phi_n. \end{aligned} \tag{1}$$

Consider the series of projections at a constant tomographic angle, i.e., $\theta_n = 45°$, and various displacement angles given by $\phi_n = (n - 1)\ (360°/N)$ where $n = 1, \ldots, N$. Geometrically, this describes the projections obtained in N-sample circular tomography. For projections corresponding to N-sample linear tomog-

raphy, the displacement angle $\phi_n = 0$ and the tomographic angles θ_n are equally spaced between $-\theta_{\max}$ and $\theta_{\max}$.

Note that the projection calculations are greatly simplified for tomographic projections. Only two arrays of numbers of dimension $(2K + 1) \times N$ containing the displacement values ($k \tan \theta_n \cos\phi_n$, $k \tan \theta_n \sin \phi_n$) are required to determine all the rays through a voxel, or alternatively all the voxels intersected by a ray. Complicated 3-D ray-tracing equations are avoided. This concept of tomographic projections is a generalization of the concentric-squares raster of Mersereau [18] and also corresponds to the weighted coaxial projections of Gordon *et al.* [4]. The procedure is general since one can interchange the i or j axis with the k axis for values of tomographic angle greater than 45°.

Each projection is composed of $L \times M$ rays that intersect various voxels as they propagate through the reconstruction volume. The ray values (raysums) are related to the densities $D(i, j, k)$ by a linear relation. A raysum $P(l, m, n)$ is given by

$$P(l, m, n) = \sum_i \sum_j \sum_k W(i, j, k, l, m, n)(D(i, j, k), \tag{2}$$

where the W are weights that correspond to the volume of intersection of a given ray and voxel. Since it is both difficult and computationally slow to evaluate the weights W exactly, an approximation is made.

$$W(i, j, k, l, m, n) = \delta(l, i - k \tan \theta_n \cos \phi_n)\delta(m, j - k \tan \theta_n \sin \phi_n) \tag{3}$$

where δ is the Kronecker delta function and $\delta(a, b) = 1$ if $a = b$ and $\delta(a, b) = 0$ if $a \neq b$. This is equivalent to the approximation made in most implementations of iterative algorithms (3). Essentially it includes only those voxels whose centers are contained within the ray. After applying this approximation, the above raysum equation reduces to

$$P(l, m, n) = \sum_{k=-K}^{K} D(l + k \tan \theta_n \cos \phi_n, m + k \tan \theta_n \cos \phi_n, k). \tag{4}$$

Note that $2K + 1$ cells contribute to each raysum (Fig. 2).

We now have a system of linear equations in which there are $L \times M \times N$ equations in $I \times J \times K$ unknowns. However, the normal methods of linear matrix algebra are not particularly useful in solving these equations. For a typical problem with 12 projections of 55×55 points and a volume of 25 sections of 55×55 points, the W matrix is of dimension $36{,}300 \times 75{,}625$. This represents a formidable task for even the largest computers. Furthermore, the problem is often underdetermined, as it is in the above example, so that a unique solution does not exist unless one specifies additional criteria such as minimum norm. For an underdetermined system of equations there are an infinite number of solutions. However, there is only one for which the magnitude (Euclidean norm) of the solution is a minimum. This is called the minimum norm solution; it also is the minimum variance solution. Tanabe [19] has shown that the ART algorithm converges to this solution. Although it has not been proved, the other iterative algorithms appear also to converge to this solution.

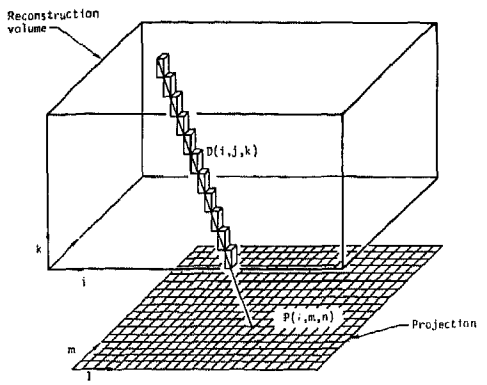

FIG. 2. Schematic representation of the reconstruction volume and a projection. The voxels shown are those intersected by the ray $P(l, m, n)$ after making the approximation given in Eq. (3).

Various iterative schemes have been developed to circumvent these difficulties. As noted, they all involve guessing at the densities $D(i, j, k)$ and calculating raysums $R(l, m, n)$ by using Eq. (4). The calculated raysums $R(l, m, n)$ then are compared to the projection data $P(l, m, n)$ and the errors are used to modify the density values. The procedure is repeated or iterated until the error terms drop below some predefined value. Summation and three iterative algorithms are now considered; the implementation for direct reconstruction from tomographic projections is briefly described below.

3.1. Summation

This algorithm, the simplest approach, does not attempt to solve the equations exactly. It is included mainly for historical reasons, because it is a digital implementation of conventional tomography.

The density of a voxel is estimated by the average of all rays through the point.

$$D(i, j, k) = \frac{1}{N'(2K+1)} \sum_n P(i - k \tan \theta_n \cos \phi_n,\ j - k \tan \theta_n \sin \phi_n,\ n), \qquad (5)$$

N' is the total number of rays intersecting the voxel and can differ from N. The factor $N'(2K + 1)$ scales the values so that the total density of the reconstruction equals the total density of a projection.

This algorithm has also been called back-projection, because it smears the rays back across the reconstruction volume. To see that it produces a blurred reconstruction, consider the reconstruction of a point. For the specific case of circular tomographic projections discussed earlier, the reconstruction consists of a point with spokes radiating out conically. In fact, the point-spread-function always is a scaled version of the projection geometry.

3.2. Algebraic Reconstruction Technique (ART)

The ART algorithm was first discovered by Kaczmarz in 1937 [20]. He discussed it as a technique for solving a system of linear equations. It was dis-

covered independently and applied to image reconstruction by Gordon and coworkers [4] and by Hounsfield [21].

Assuming that estimates of the densities $D(i, j, k)$ exist, the raysums can be calculated as before

$$R^{q,n}(l, m, n) = \sum_{k=-K}^{K} D^{q,n}(l + k \tan \theta_n \cos \phi_n, m + k \tan \theta_n \sin \phi_n, n). \quad (6)$$

The superscript q, n refers to the qth iteration and the nth projection. The error term of any ray is

$$E^{q,n}(l, m, n) = P(l, m, n) - R^{q,n}(l, m, n). \quad (7)$$

The ray equation can be satisfied by adding the corrections to the $D(i, j, k)$ along the ray such that the sum of the corrections equals $E^{q,n}(l, m, n)$. Since no a priori knowledge exists regarding the source of the error, it is equally distributed to each voxel along the ray. Hence, the density at the voxel is changed according to

$$D^{q+1,n}(i, j, k) = D^{q,n}(i, j, k) + \frac{1}{(2K + 1)} E^{q,n}(i - k \tan \theta_n \cos \phi_n, j - k \tan \theta_n \sin \phi_n, n). \quad (8)$$

All rays in a given projection are considered in turn, then other projections are chosen and the procedure is repeated for each. The raysum equations are satisfied only for the last projection used because changing the density values disturbs the raysums of other projections. Therefore, the entire process is repeated until some chosen error criterion is satisfied.

3.3. Simultaneous Iterative Reconstruction Technique (SIRT)

SIRT (5) is a modification of ART that uses data from all the projections simultaneously. The value of a voxel is modified by the average error of all rays through the voxel

$$D^{q+1}(i, j, k) = D^{q}(i, j, k) = \frac{1}{N'(2K + 1)} \sum_{n} E^{q}(i - k \tan \theta_n \cos \phi_n, j - k \tan \theta_n \sin \phi_n, n). \quad (9)$$

The factor $1/N'(2K + 1)$ distributes the error equally among all the points contributing to the summation. Note that the correction term corresponds to back-projecting the raysum errors.

3.4. Iterative Least Squares Technique (ILST)

Goitein [6] derived an algorithm that minimizes the mean square error (residual) between the calculated raysums and measured projections. The residual after the qth iteration is defined by

$$\Re^{q} = \sum_{l} \sum_{m} \sum_{n} [P(l, m, n) - R^{q}(l, m, n)]^2 / \sigma^2(l, m, n), \quad (10)$$

where $\sigma^2(l, m, n)$ is the variance of the noise in the l, m, nth ray. In this imple-

mentation, it is assumed that the noise is additive with uniform variance. By following the derivation of Budinger and Gullberg [2] but using this assumption instead of their assumption of Poisson statistics, we arrive at the formula for the change in density

$$\Delta D^q(i, j, k) = D^{q+1}(i, j, k) - D^q(i, j, k)$$

$$= \frac{1}{N'} \sum_n E^q(i - k \tan \theta_n \cos \phi_n, j - k \tan \theta_n \sin \phi_n, n). \quad (11)$$

Note that this algorithm initially assigns all the error to the voxel under consideration. Hence, the sum of the changes will exceed the sum of the errors and produce diverging behavior. Therefore, a damping factor β is introduced. It is chosen to minimize the mean square error between the new raysums and the projections

$$R^{q+1}(l, m, n) = \sum_k [D^q(l + k \tan \theta_n \cos \phi_n, m + k \tan \theta_n \sin \phi_n, k) + \beta \Delta D^q(l + k \tan \theta_n \cos \phi_n, m + k \tan \theta_n \sin \phi_n, k)]. \quad (12)$$

Again following the derivation of Budinger and Gullberg, one obtains

$$\beta = \sum_l \sum_m \sum_i [E^q(l, m, n) \sum_k \Delta D^q(l + k \tan \theta_n \cos \phi_n, m + k \tan \theta_n \sin \phi_n, k)] /$$

$$\sum_l \sum_m \sum_n [\Delta D^q(l + k \tan \theta_n \cos \phi_n, m + k \tan \theta_n \sin \phi_n, k)]^2. \quad (13)$$

Each of the algorithms as presented is unconstrained, in that negative density values are permitted. Since density values cannot be negative, a constraint requiring the calculated value to be nonnegative can be introduced. Let $\tilde{D}^q(i, j, k)$ be the adjusted density after the qth iteration; the constrained density value $D^q(i, j, k)$ is given by

$$D^q(i, j, k) = \max[0, \tilde{D}^q(i, j, k)]. \quad (14)$$

An algorithm using this procedure is partially constrained. A fully constrained algorithm would also require the density to be less than some maximum value.

4. EXPERIMENT AND RESULTS

4.1. Computer-Generated Synthetic Images

In order to avoid the problems associated with testing algorithms on pseudoprojection (consistent) data a computer program to generate synthetic test images was written. The program calculates analytically the projections of spheres for specified angles (θ_n, ϕ_n). Calculation of the projections using the raysum equations generates data consistent with the equations and thus does not permit one to check the validity of the approximations associated with the weights W. Reconstructions using pseudoprojection data are generally more exact than those using analytically calculated or experimental data. Random

noise with either uniform or Gaussian distribution can be added to the projections. The program also generates test images or "ideal" reconstructions [5] to be used for comparison with the reconstructions. To test the algorithms, three series of projections were generated. In each, the reconstruction volume was partitioned into 25 sections of 85 × 85 points. The projections were digitized to 55 × 55 points.

The first test series consists of two spheres surrounded by a shell. The shell is set at density 150 and the spheres at density 125 and 175. The outer radius of the shell is 11 units and the radius of each sphere is 2 units. The background density is 50. Thus, the mean object-to-background density is 3 to 1, corresponding roughly to the density range for stained biological material as viewed by electron microscopy. In the second test series, there are nine spheres of different size and density. The densities range from 45 to 95 and the radii from 2 to 7 units with the background density set at 20. A third series consists of uniform gray projections to which random noise was added. The noise is Gaussian distributed with zero mean and coefficient of variation equal to 5, 10, and 20%. The coefficient of variation is the standard deviation expressed as percent of the mean.

The choice of reconstruction volume deserves some consideration. An extended field, in which the i and j dimensions are greater than the corresponding projection dimensions, is required if every projection does not include the entire object under study, i.e., if outer rays are excluded from the field of view. Such situations arise in the electron microscopy of tissue sections if only a subarea is being reconstructed and in nuclear medicine if the field of view of a scintillation camera is less than the width of the patient. For such extended fields, the reconstruction volume consists of three regions (Fig. 3). All the voxels in the central region are intersected by the same number of rays, voxels in region 2 are intersected by a variable number of rays, and voxels in region 3 are not intersected by any rays. Note the problems that could arise if other choices were made. For example, if the size of the reconstruction section was equated to the projection size, any density occur-

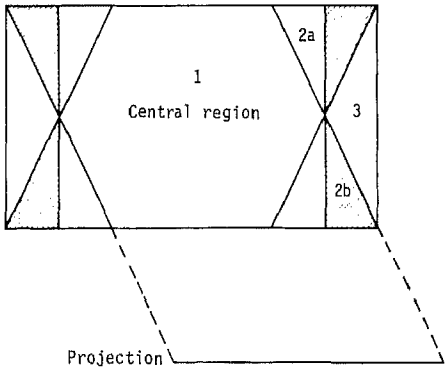

FIG. 3. Reconstruction volume showing the extended field. All the voxels in the central region (region 1) are intersected by the same number of rays; voxels in region 2 are intersected by a varying number of rays; and voxels in region 3 are not intersected by any rays. Densities in region 2b (shaded) would be "folded back" if the extended field were not used.

ring in region 2b could be "folded back" into the central region. Of course, the reconstruction is only meaningful in the central region.

All the reconstruction calculations were done on a CDC-7600 computer using integer arithmetic. Considerable savings in computer memory were obtained by storing the reconstruction, projections, and some of the auxiliary arrays as 12-bit words, 5 to each 60-bit computer word.

Several error measures can be used to evaluate the reconstructions. Detailed discussions of most of the criteria are given in Herman [22]. Since discrepancy, a normalized Euclidian distance function, was found to be the most useful measure of performance, it is the only one used in this paper. Discrepancy is defined as

$$\delta(q) = [\sum_i \sum_j \sum_k (D^q(i, j, k) - T(i, j, k))^2 / \sum_i \sum_j \sum_k (T(i, j, k) - \bar{T})^2]^{\frac{1}{2}}, \quad (15)$$

where D^q is the reconstruction density at iteration q, T is the density of the test image, and $\bar{T}$ is the mean density of the test image. The numerator is the root-mean-square error and the denominator is the standard deviation of the test picture. A value greater than one indicates that a uniform gray image is closer to the test image than is the reconstruction.

The results of three experiments are now presented. In the accompanying illustrations, the reconstructions are represented only by the central 55×55 points of each section. The sections are displayed left to right and top to bottom so a three-dimensional object can be constructed by stacking the sections. Each picture was scaled and displayed with 64 gray levels so the contrast varies depending on the maximum value. For the iterative algorithms 15 iterations were calculated.

4.2. Comparison of 2-D and 3-D Reconstruction

Two projection geometries are compared for the partially constrained SIRT algorithm. The linear case consists of 12 projections equally spaced between $\pm 45°$. This geometry is particularly interesting because it yields projections that correspond to the weighted coaxial projections of Gordon *et al.* [4] and the concentric-squares raster of Mersereau [18]. Hence one can compare direct 3-D reconstruction with serial 2-D reconstruction using the same test images. The circular case consists of 12 projections at a displacement angle of 30° and a tomographic angle of 45°. The reconstruction of the shell-surrounded spheres by these two projection geometries are shown in Figs. 4a and 4b. Fifteen iterations were calculated. Both reconstructions give what appear to be blurred approximations of the original. The shell and spheres are clearly delineated in each; the reconstruction using the circular projections has better definition with a less pronounced background artifact. The shell extends into the upper and lower sections indicating an elongation in the vertical (k axis) direction. The elongation is greater for the reconstruction using the linear projections (Fig. 4a), since for this reconstruction the two spheres are also visible in the central section. Note that for the linear projections, some sections of the shell do not appear circular, particularly in the top and bottom sections. The same general comments also

TABLE 1

Discrepancy Measures for Linear and Circular Geometries[a]

Geometry	Shell-surrounded spheres	Multiple spheres
Linear	0.77	0.75
Circular	0.61	0.65

[a] Values are after 15 iterations of SIRT.

apply to the reconstructions of the multiple spheres test series. Both reconstructions are blurred approximations of the original. With the linear projections (Fig. 4c) there is considerable elongation of the spheres in the vertical direction, an artifact that is less pronounced with the circular projections (Fig. 4d).

Discrepancy measures for these reconstructions are given in Table 1. For both test series the discrepancy is lower for the reconstruction from circular projections, indicating a more exact reconstruction. A value of zero corresponds to complete agreement; it is not obtained in practice because of the approximations made in deriving the weights. As noted earlier, a value greater than one indicates that a uniform gray image is a better approximation to the test image than is the reconstruction.

4.3. Number of Projections

The effect of the number of projections on the quality of the reconstructions is examined using the partially constrained SIRT algorithm and considering 6, 12, 18, and 24 synthetic circular projections. All projections are at a tomographic angle of 45°. The reconstructions for the shell-surrounded spheres are shown in Fig. 5. The shell and spheres are visible in each reconstruction but are better delineated as the number of projections increases. The leaf pattern that appears as a background artifact results from using a limited number of projections; it decreases with increasing number of projections. Similar results are obtained with the multiple spheres test series (not shown). Discrepancy values for these reconstructions are given in Table 2. For both test series, the largest decrease in value

TABLE 2

Discrepancy Measures vs Number of Projections[a]

No. of projections	Shell-surrounded spheres	Multiple spheres
6	0.66	0.67
12	0.61	0.65
18	0.60	0.65
24	0.59	0.65

[a] Values are after 15 iterations of SIRT.

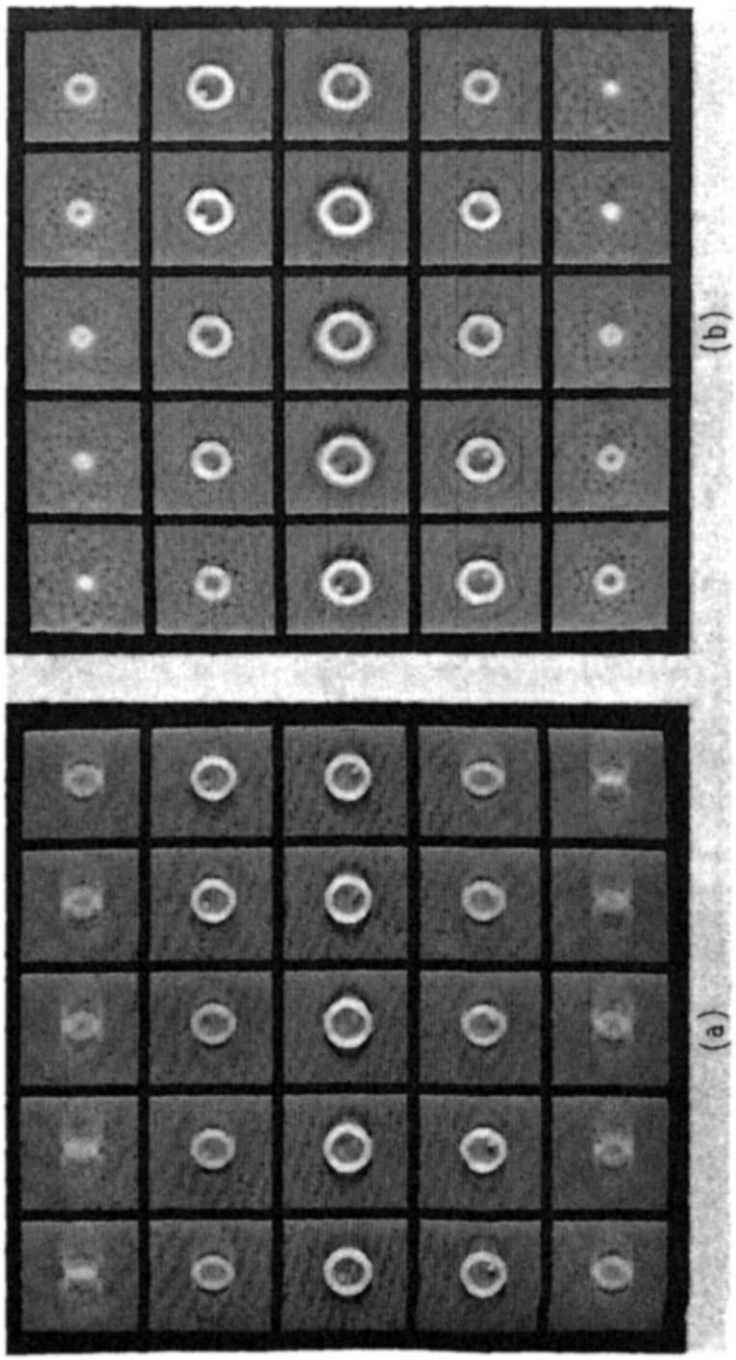
(b)
(a)

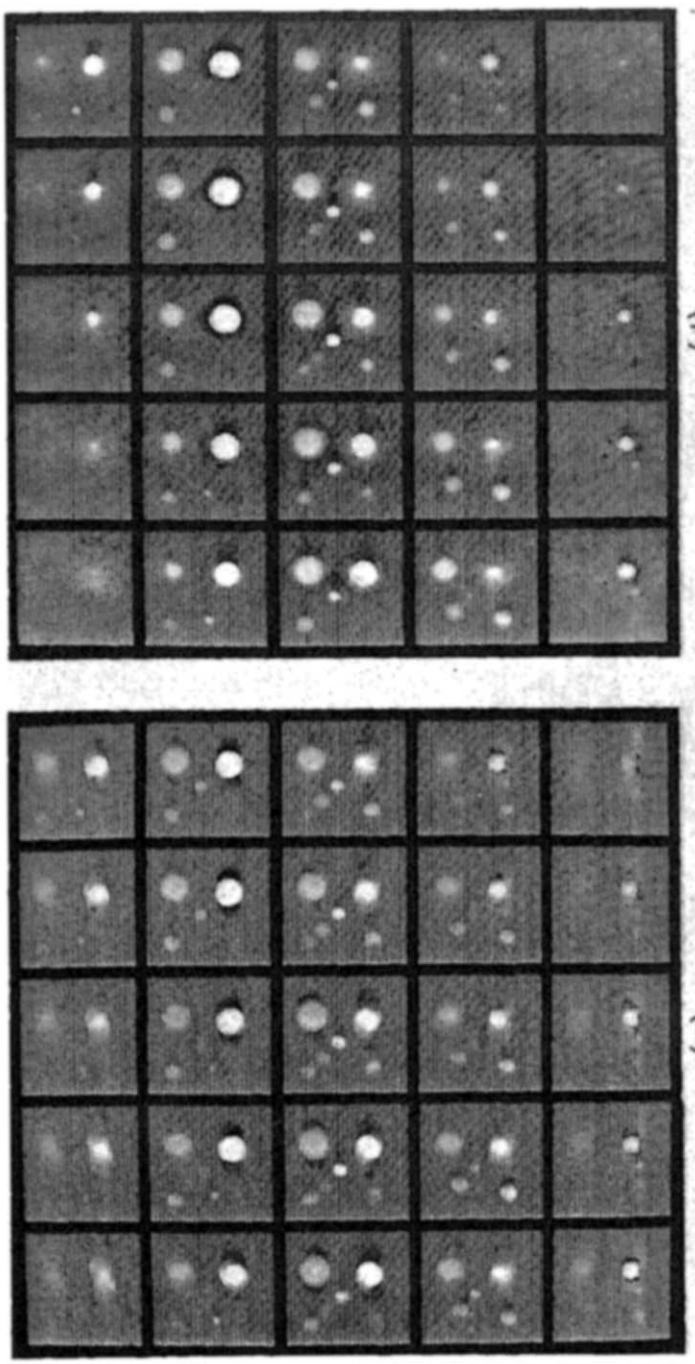

FIG. 4. Reconstructions for linear and circular projections: (a) reconstruction of shell-surrounded spheres from linear projections; (b) reconstruction of shell-surrounded spheres from circular projections; (c) reconstruction of multiple spheres from linear projections; (d) reconstruction of multiple spheres from circular projections. All reconstructions are after 15 iterations of SIRT. The reconstructions consist of 25 sections of 85 × 85 points. Only the central 55 × 55 points of each section are displayed; the sections are displayed left to right and top to bottom.

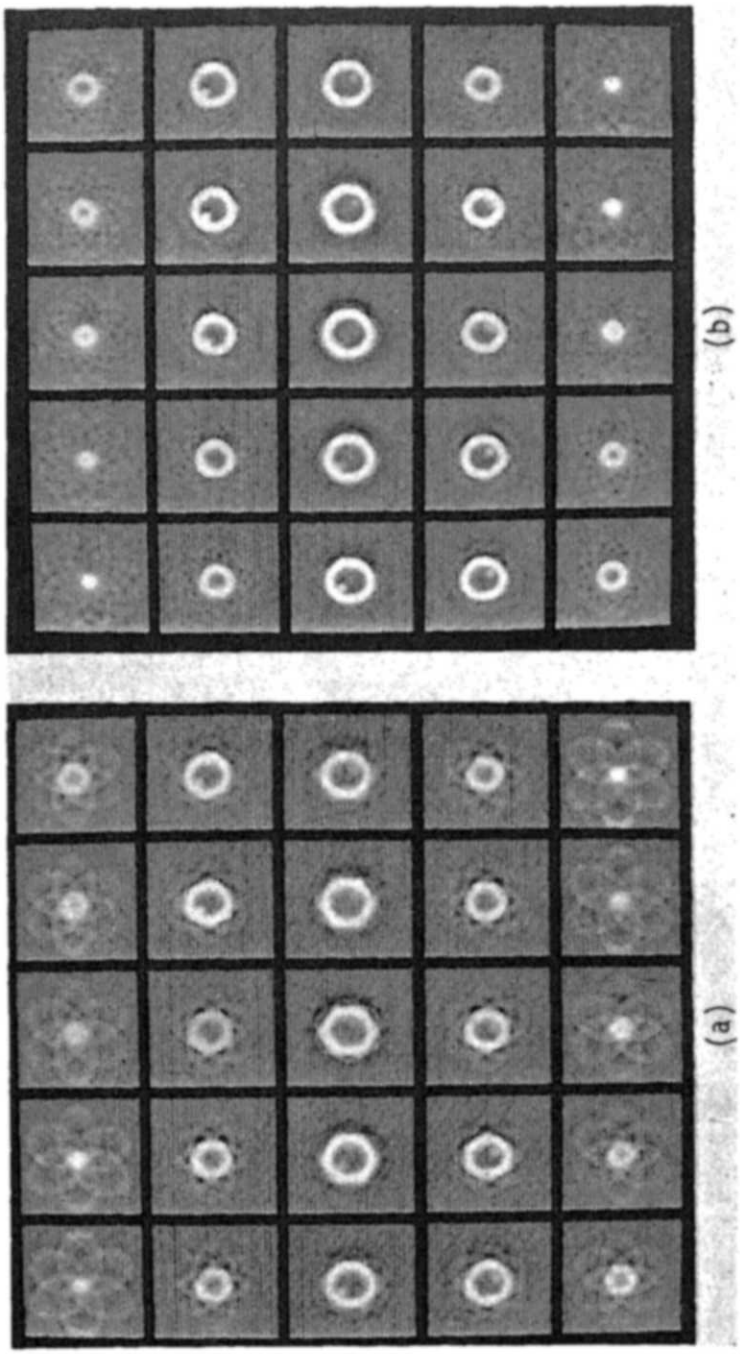
(b)
(a)

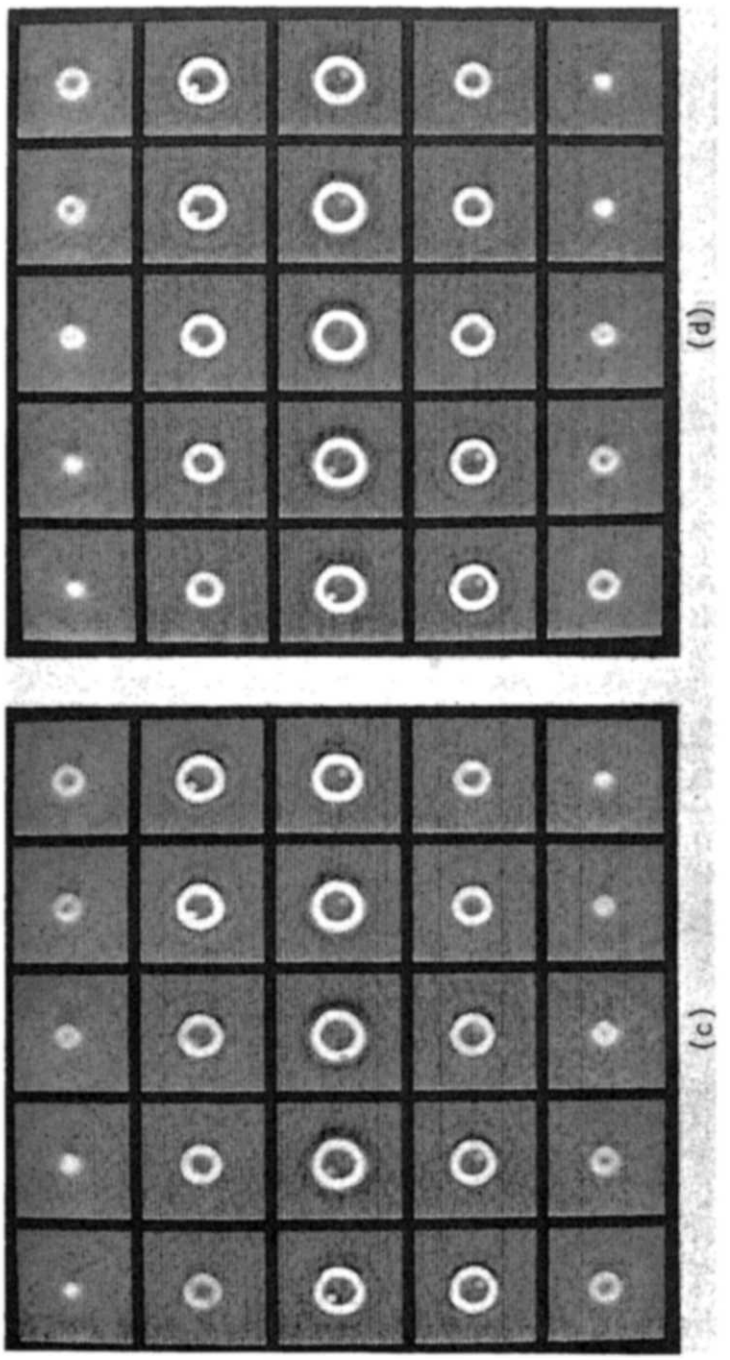

FIG. 5. Reconstructions of the shell-surrounded spheres for a variable number of circular projections: (a) 6 projections; (b) 12 projections; (c) 18 projections; and (d) 24 projections. All reconstructions are after 15 iterations of SIRT. Note the decrease in the background leaf pattern with increasing number of projections.

TABLE 3

Computer Time (One Iteration) and Memory Requirements of the Four Algorithms

Algorithm	Computer time (sec)	Computer storage requirements		
		Reconstruction arrays	Projection arrays	Total 60-bit words
Summation	3.0	1	1	43,385
ART	11.8	1	1.1[a]	44,111
SIRT	5.4	1	2	50,645
ILST	8.8	2	3	94,030

[a] ART actually requires only $1 + 1/N$ where N is the number of projections.

occurs between 6 and 12 projections; little improvement is obtained by adding additional projections.

4.4. *Comparison of Algorithms*

The performance of the four algorithms summation, ART, SIRT, and ILST are compared using the three series of synthetic images described above. Each series consisted of 12 projections with a displacement angle of 30° and a tomographic angle of 45°.

The computer execution times and memory requirements for the algorithms are given in Table 3; the times are for one iteration of the algorithm. Total time, a more important parameter, depends on the number of iterations required for convergence. An indication of this parameter can be obtained by plotting discrepancy as a function of iteration (see Fig. 6). The ART algorithm, although the slowest per iteration, converges in the fewest iterations. However, these times are very much computer and programmer dependent. The long iteration time for the ART algorithm results from randomly accessing the byted reconstruction array.

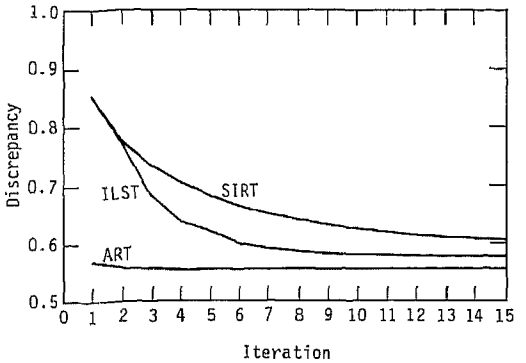

FIG. 6. Convergence of the iterative algorithms is indicated by plotting discrepancy as a function of iteration number. The ART algorithm converges in the fewest iterations; SIRT requires the most iterations for convergence. Discrepancy is the root-mean-square error between the reconstruction and the test image normalized to the standard deviation of the test image.

It is not a problem if the array is accessed sequentially which is the case for the other algorithms. Storage requirements are specified by enumerating for each algorithm all of the arrays equal in dimension to the reconstruction and projection arrays (Table 3). The total storage requirements in 60-bit computer words are given also. The storage requirements of summation, ART, and SIRT are comparable; ILST requires approximately twice the memory of the other algorithms.

The algorithms are partially constrained for the shell-surrounded spheres and multiple spheres test series but are unconstrained for the noisy-test series. For the iterative algorithms, the initial guess is taken to be the reconstruction using summation. This differs from the procedure described previously [23]. Setting all voxels to zero or to the average density produces equivalent results with one exception. The ART algorithm with an extended field produces disturbing edge effects if the initial guess is zero.

The reconstructions for the shell-surrounded spheres are shown in Fig. 7. All the algorithms gave reconstructions that appear to be blurred approximations of the original. The shell extends into the upper and lower sections indicating an elongation in the vertical direction. The two inner spheres are clearly delineated by the three iterative algorithms, but not by summation. The reconstruction using ART shows the most detail. There appears to be little difference between SIRT and ILST in the quality of reconstruction, although the 12-leaf pattern around the shell is more pronounced in the ILST reconstruction. This pattern is a low-intensity artifact that results from the limited number of views; it can be removed by varying the threshold for the image. Discrepancy values for the reconstructions are given in Table 4. For the iterative algorithms, the values are for the 15th iteration. The measure confirms the visual interpretation of the reconstructions; the ART reconstruction has the lowest value, the ILST is the next best. The values for summation are considerably higher than those for the iterative algorithms.

The reconstructions for the multiple-spheres test object is shown in Fig. 8. In general, the comments about the shell-surrounded spheres apply to this series also. All the algorithms produced blurred approximations of the original; summation gave the most blurring. The reconstruction using ART showed the most detail. Again, the background artifacts were less pronounced with SIRT than with ILST. The discrepancy measures are given in Table 4. This measure pre-

TABLE 4

Discrepancy Measures for Algorithms

Algorithm	Shell-surrounded spheres	Multiple spheres
Summation	0.85	0.88
ART	0.56	0.63
SIRT	0.61	0.65
ILST	0.58	0.64

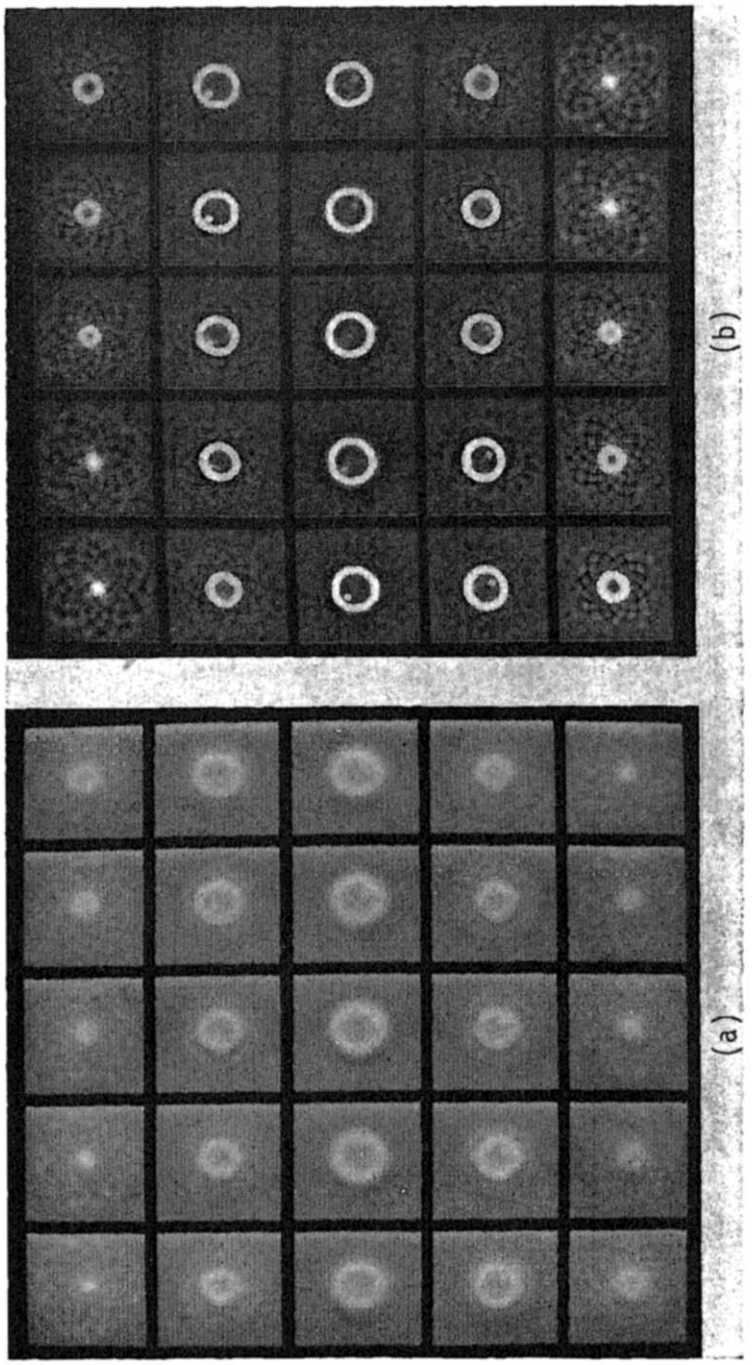
(b)
(a)

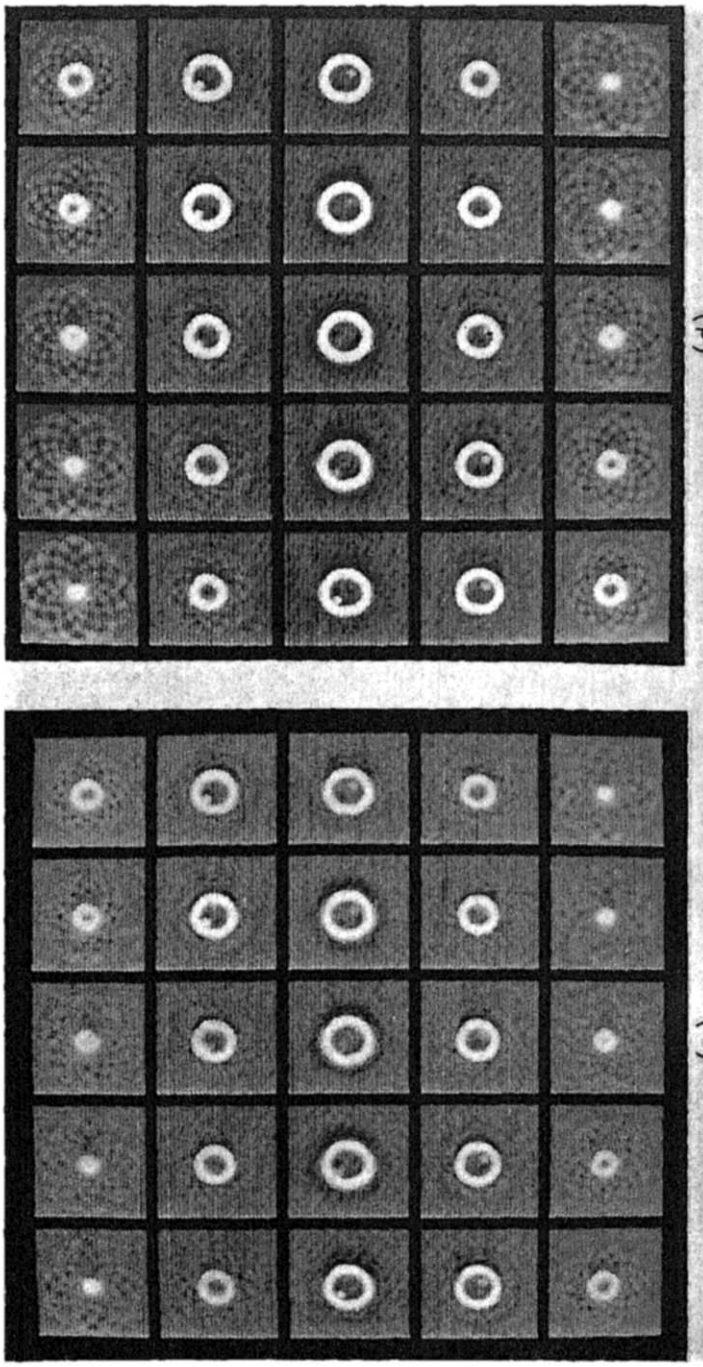

FIG. 7. Reconstructions of the shell-surrounded spheres for the four algorithms: (a) summation; (b) ART; (c) SIRT; and (d) ILST. For the iterative algorithms 15 iterations were calculated. All the algorithms gave reconstructions that appear to be blurred approximations of the original. The shell extends into the upper and lower sections indicating an elongation in the vertical direction. (The outer radius is 11 units so it should not appear in these sections.) The two inner spheres are clearly delineated by the three iterative algorithms but not by summation.

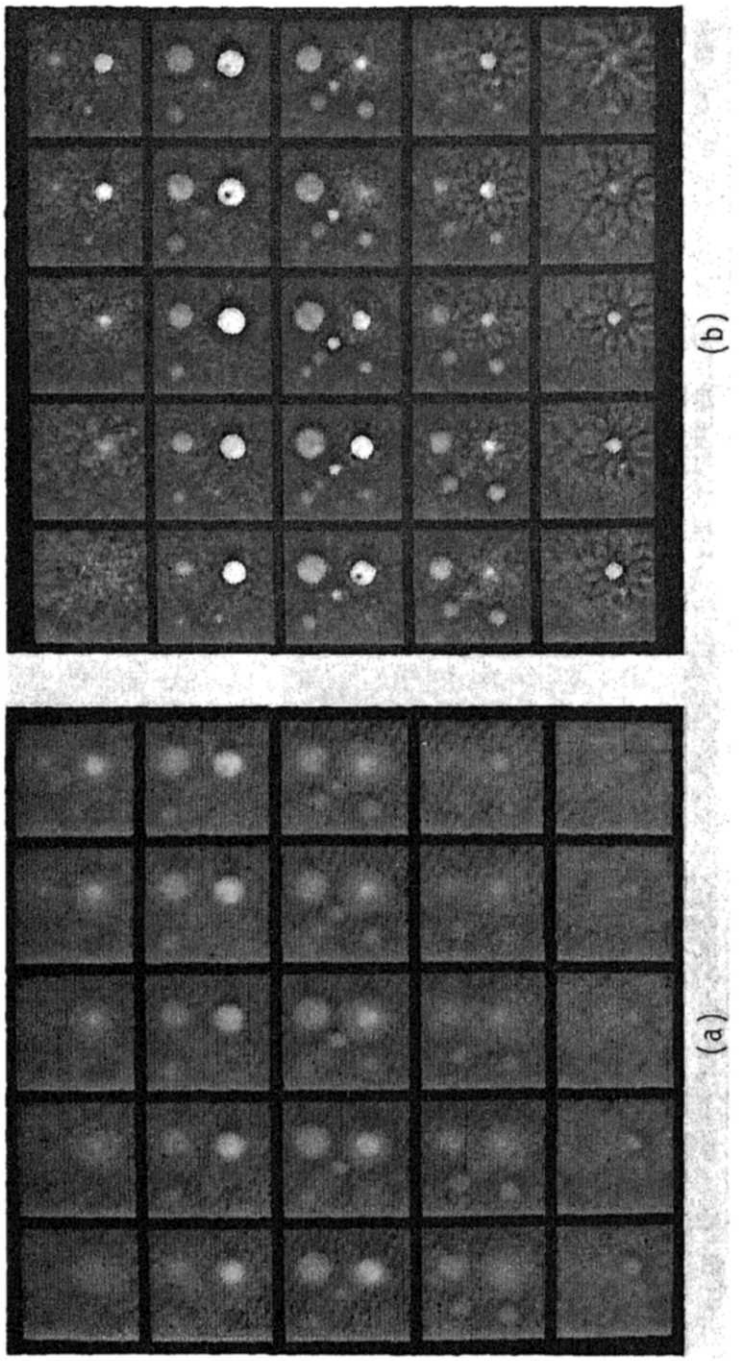
(b)
(a)

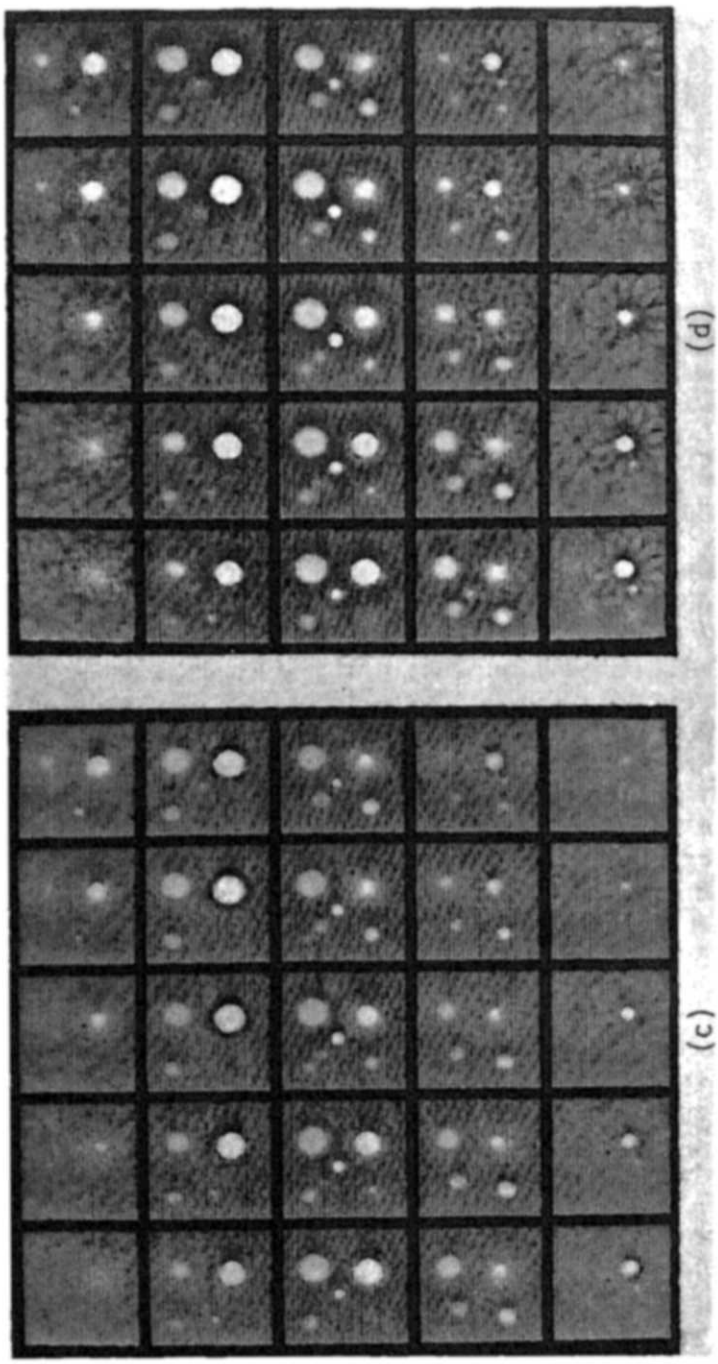

FIG. 8. Reconstructions of the multiple spheres for the four algorithms: (a) summation; (b) ART; (c) SIRT; and (d) ILST. For the iterative algorithms 15 iterations were calculated. All the algorithms produced blurred approximations of the original; summation gave the most blurring. The reconstruction using ART showed the most detail; the hole in one of the spheres is most visible for this algorithm.

TABLE 5

Noise Amplification Factor of Reconstructions Using Noisy Projections[a]

Algorithms	Noise amplification factor[b]		
	5%	10%	20%
Summation	0.30	0.33	0.30
ART	2.62	3.43	—[c]
SIRT	0.58	0.84	1.36
ILST	0.98	2.20	—[c]

[a] The noise amplification factor is the ratio of the coefficients of variation for the reconstructions and projections. For the iterative algorithms, values are after 15 iterations.

[b] The three different noise levels are expressed as coefficients of variation (C.V.) of the projection.

[c] Since noise for a lower noise level was amplified, this value was not calculated.

ferred ART, but the difference between it and the other iterative algorithms is not as great for this test series.

The noisy-test series was used to deduce the effects of noise on the algorithms. For unconstrained algorithms the reconstruction process is a linear operation and the effects of additive noise can be considered separately. This can be accomplished by inputting projection data consisting of pseudorandom Gaussian variables superimposed on a uniform background level. The coefficient of variation of the reconstruction is then a numerical factor by which the noise in the projections is increased or decreased by a given algorithm. Table 5 presents the noise amplification factor which is defined as the C.V. (coefficient of variation) of the reconstruction divided by the C.V. of the projections; values greater than one indicate noise amplification. With summation and SIRT, the noise level of the reconstruction is better than that of the projections, except that SIRT amplified the 20% noise. The ILST performed well for the 5% noise but amplified the 10% noise. ART amplified projection noise at both levels tested.

5. DISCUSSION AND CONCLUSIONS

This paper considers several aspects of the problem of performing direct three-dimensional reconstruction. In particular, iterative algorithms are extended to perform reconstructions from tomographic projections and an experimental investigation uses computer-generated synthetic images to compare the techniques. Rather than employ coaxial projections for their computational simplicity, it was decided to use true three-dimensional data. This posed a complex computational problem, but it offered several advantages, principally by increasing the flexibility of data acquisition. For the particular method of data collection employed (tomographic projections), the iterative algorithms appeared to be the most promising since they are the easiest to adapt to this projection geometry. Although it has not been demonstrated in this context, it appears that additional constraints could be introduced into this algebraic formulation. For example, Kashap and Mittal [24] consider minimum norm and continuity. Another

possible constraint is maximum entropy. This may be useful for underdetermined systems.

An experimental investigation was undertaken, because there is no acceptable theoretical basis on which to compare the techniques. This investigation consisted of three separate experiments. In the first experiment, reconstructions from circular projections were shown to be superior to the reconstructions from linear projections, verifying the hypothesis that true 3-D reconstruction is useful when the range of viewing angles is limited. This is not surprising, since circular projections span a wider range than the linear projections and hence introduce more "independent" information. This agrees with observations using coaxial projections [25] in which it was found that the range of viewing angles is more important than the number of views.

The superiority of circular projections is important for several applications in which the range of viewing angles is limited. Even though tilting stages capable of 180° rotation have been constructed for electron microscopes, views at large angles of tilt are useless since the electron beam intersects the supporting grid. Also, experimental setups in holographic interferometry that allowed a 180° angle of view would be very complex and require numerous optical components. In addition, if an enclosed test cell is required, it is a formidable task to design a cell which does not introduce severe optical distortions and which avoids multiple reflections at the glass/air interface. In these cases it is more important to devise reconstruction schemes that make maximum use of the available information and forgo the computational simplicity of coaxial projections.

In the second experiment, reconstructions were done from a varying number of projections. The purpose was to determine the number of views required for a satisfactory reconstruction and in some sense to determine the resolution of the reconstruction. For the quantization used in the reconstruction, 12 views seem sufficient; little detail is gained with additional projections. However, this experiment does not directly address the question of resolution. Since there is blurring in the vertical direction, the resolution is obviously not isotropic. Furthermore, simply stating that spheres of a certain diameter appear in the reconstruction is also unsatisfactory, since their appearance or nonappearance depends on the contrast and complexity of the image. An appropriate experiment would permit frequency limits to be specified and the results to be expressed in terms of the system transfer function.

Finally, reconstructions were also calculated by means of four different algorithms. The results obtained are subject to many interpretations depending on the application and its requirements. Summation always produced a blurred image and is generally not considered useful for digital reconstruction. It can be implemented more conveniently by analog methods, as it is in radiography. The ART requires the least computer memory and converges in the fewest iterations. However, it is very sensitive to noise. Modifications of the ART algorithm to handle noise have been made by Herman [26], but they were not implemented for 3-D reconstruction. Further testing of the ART algorithm with these modifications might be justified where computer storage is a problem.

The reconstructions using the SIRT and ILST algorithms were similar, with

the discrepancy measure favoring ILST. Nonetheless, there are two reasons for favoring SIRT: It requires considerably less computer memory than ILST and performs considerably better with the noisy-test series. Since many applications deal with noisy projection data, this is perhaps an overriding reason for preferring the SIRT algorithm.

The methodology developed for these analyses can be extended to any reconstruction algorithm. Proper testing of any new algorithm requires procedures similar to those employed in this investigation. At a minimum, test objects representative of the objects one encounters in practice should be reconstructed for varying numbers of projections, projection geometries, and noise levels. The importance of noise cannot be overestimated. Other experimental conditions as determined by the application should also be considered.

Since many existing experimental setups can collect tomographic projections, the reconstruction methods developed here for synthetic images can be extended to electron microscopy, nuclear medicine, and other applications of practical importance.

ACKNOWLEDGMENT

The author gratefully acknowledges the helpful advice and criticism provided by Dr. Brian H. Mayall, of the Biomedical and Environmental Research Division, Lawrence Livermore Laboratory. Reference to a company or product name does not imply approval or recommendation of the product by the University of California or the U.S. Energy Research and Development Administration.

REFERENCES

1. J. Radon, Über die Bestimmung von Funktionen durch ihre Integralwerte langs gewisser Mannigfaltigkeiten, *Ber. Akad. Wiss. (Leipzig) Math. Phys. Klass.* 69, 1917, 262–277.
2. T. F. Budinger and G. T. Gullberg, Three-dimensional reconstruction in nuclear medicine emission imaging, *IEEE Trans. Nucl. Sci.* NS-21, 1974, 2–20.
3. R. Gordon and G. T. Herman, Three-dimensional reconstruction from projections: A review of algorithms, *Intern. Rev. Cytol.* 33, 1974, 111–151.
4. G. Gordon, R. Bender, and G. T. Herman, Algebraic reconstruction techniques (ART) for three-dimensional electron microscopy and x-ray photography, *J. Theoret. Biol.* 29, 1970, 471–481.
5. P. F. C. Gilbert, Iterative methods for the three-dimensional reconstruction of an object from projections, *J. Theoret. Biol.* 36, 1972, 105–117.
6. M. Goitein, Three-dimensional density reconstruction from a series of two-dimensional projections, *Nucl. Instrum. Meth.* 101, 1971, 509–518.
7. R. G. Hart, Electron microscopy of unstained biological material: The polytropic montage, *Science* 159, 1968, 1464-1467.
8. C. B. Lim, D. Chu, L. Kaufman, V. Perez-Mendez, and J. Sperinde, Characteristics of multiwire proportional chambers for positron imaging, *IEEE Trans. Nucl. Sci.* NS-21, 1974, 85–88.
9. H. H. Chau and O. S. F. Zucker, Holographic thin-beam reconstruction technique for the study of 3-D refraction-index field, *Opt. Commun.* 8(4), 1973, 336–339.
10. D. G. Luenberger, *Optimization by Vector Space Methods*, Wiley, New York, 1969.
11. P. Edholm, The tomogram: Its formation and content, *Acta Radiol. Suppl.* 193, 1960.
12. R. A. Crowther, D. J. DeRosier, and A. Klug, The reconstruction of a three-dimensional

structure from projections and its application to electron microscopy, *Proc. Roy. Soc. (London) Sec. A* **317**, 1970, 319–340.
13. D. G. Grant, Tomosynthesis: A three-dimensional radiographic imaging, *IEEE Trans. Biomed. Eng.* **BME-19**, 1972, 20–28.
14. R. G. Hart and J. Yoshiyama, Polytropic montage: Ribosomes examined in tissue section, *Proc. Nat. Acad. Sci. U.S.A.* **65**, 1970, 402–408.
15. R. A. Crowther and A. Klug, Structural analysis of macromolecular assemblies by image reconstruction from electron micrographs, *Ann. Rev. Biochem.* **44**, 1975, 161–182.
16. P. T. Radulovic and C. M. Vest, Direct three-dimensional reconstruction, *Digest of Papers, Image Processing for 2-D and 3-D Reconstruction from Projections; Theory and Practice in Medicine and the Physical Sciences*, Stanford University, Palo Alto, California, August 4–7, 1975.
17. P. Schmidlin, Iterative separation of sections in tomographic scintigrams, *Nucl. Med.* **11**, 1972, 1–16.
18. R. M. Mersereau, Recovering multidimensional signals from their projections, *Computer Graphics Image Processing* **1**, 1973, 179–195.
19. K. Tanabe, Projection method for solving a singular system of linear equations and its applications, *Numer. Math.* **17**, 1971, 203–214.
20. M. S. Kaczmarz, Angenaherte Auflösung systemen linearer Gleichungen, *Acad. Polon. Sci. Lett. Bull. A* **3**(3), 1937, 355–357.
21. G. N. Hounsfield, A method of and apparatus for examination of a body by radiation such as x or gamma radiation, *The Patent Office, London*, Patent Spec. 1283915, 1972.
22. G. T. Herman, Two direct methods for reconstructing pictures from their projections: A comparative study, *Computer Graphics Image Processing* **1**, 1972, 123–144.
23. J. G. Colsher and R. G. Hart, Comparison of algorithms for three-dimensional image reconstruction from a series of conical projections, *Digest of Papers, Topical Meeting on 2-D and 3-D Reconstruction from Projections, Theory and Practice in Medicine and the Physical Sciences*, Stanford University, Palo Alto, California, August 4–7, 1975.
24. R. L. Kashap and M. C. Mittal, Picture reconstruction from projections, *IEEE Trans. Computers* **C-24**, 1975, 915–923.
25. J. G. Colsher, unpublished.
26. G. T. Herman, A relaxation method for reconstructing objects from noisy x-rays, *Math. Programming* **8**, 1975, 1–19.